

Supporting information

The high activity of step sites on Pd nanocatalysts in electrocatalytic dechlorination

Yao-yin Lou,^{a,†,*} Chi Xiao,^{a,†} Jiayi Fang,^a Tian Sheng,^b Lifei Ji,^a Qizheng Zheng,^a Bin-Bin Xu,^a Tian Na,^{a,*} and Shi-Gang Sun^{a,*}

^a State Key Laboratory of Physical Chemistry of Solid Surfaces, Department of Chemistry, College of Chemistry and Chemical Engineering, Xiamen University, Xiamen, 361005, China

^b College of Chemistry and Materials Science, Anhui Normal University, Wuhu, 241000, P. R. China

[†]Y.Y. Lou and C. Xiao contributed equally to this work

Table S1. SWP treatments of Pd NCs on GC and CP

Electrodes		C_{PdCl_2} (mM)	E_N (V)	t_N (ms)	E_L (V)	E_U (V)	Miller indices	d_{step} ($\times 10^{14}$)
GC substrate	Cubic Pd{100} NCs	0.2	-0.1	20	0.3	0.61	{100}	/
	THH Pd{310} NCs	0.2	-0.1	20	0.3	0.71	{310}	4.18
CP substrate	Cubic Pd{100} NCs	0.8	-0.2	140	0.3	0.51	{100}	/
	THH Pd{310} NCs	0.8	-0.2	140	0.3	0.73	{310}	4.18

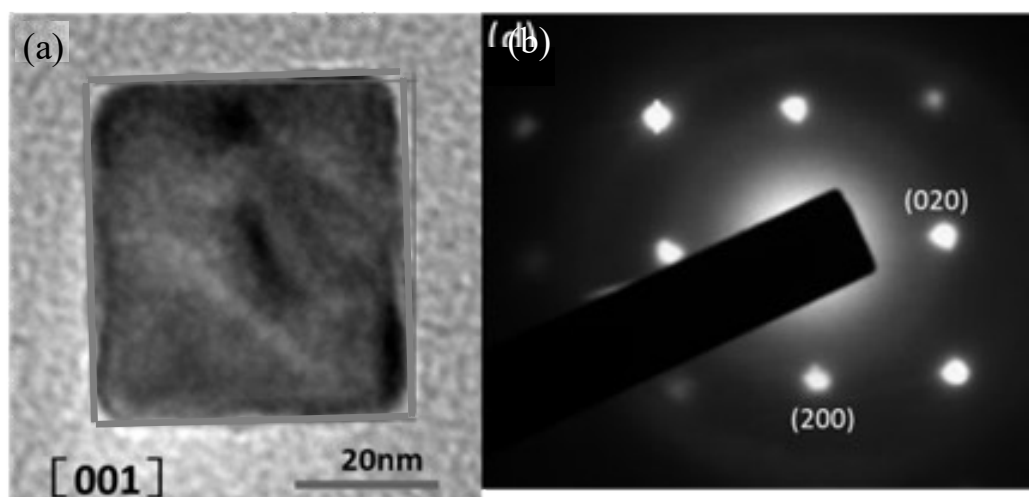


Figure S1. TEM (a) and the corresponding SAED pattern (b) of the obtained cubic Pd{100} nanocrystals along [001] direction. The electrochemical synthesis was conducted at $E_N = -0.10$ V, $t_N = 0.02$ s, $E_L = 0.30$ V, $E_U = 0.61$ V, $f = 100$ Hz, and with growth time $t_{\text{growth}} = 45$ min, in 0.2 mM PdCl₂ + 0.1 M HClO₄ solution.

The atomic arrangements of the facets of the as-prepared THH Pd{310} NCs can be illustrated as {100} terrace(s) followed by {110} step(s) periodically; and those arrangements were controlled by varying the E_U of the SWP¹. Normally, the steps sites along with kink and ledge sites were considered as the active sites for bond cleavage proved by single crystal electrode studies².

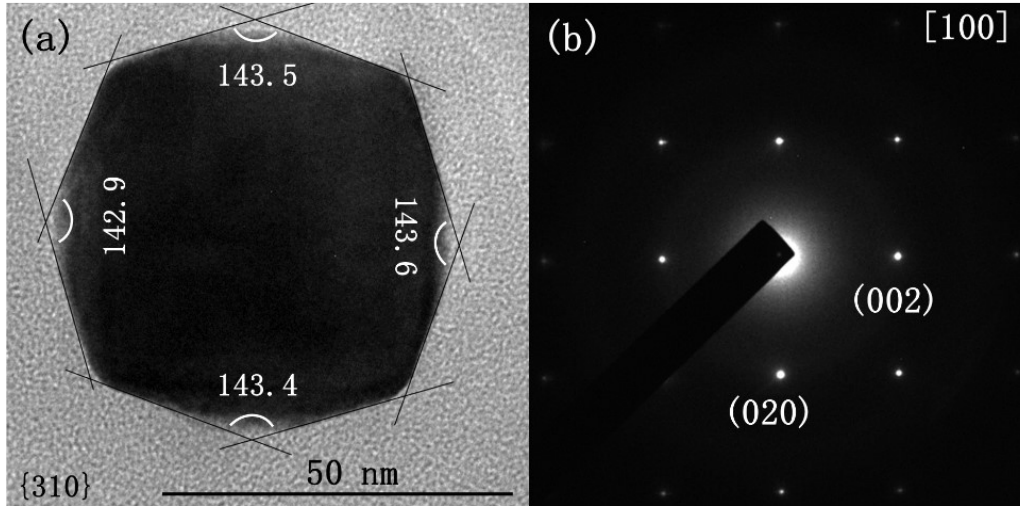


Figure S2. TEM (a) and the corresponding SAED pattern (b) of the obtained THH Pd{310} nanocrystals along [001] direction. The electrochemical synthesis was conducted at $E_N = -0.10$ V, $t_N = 0.02$ s, $E_L = 0.30$ V, $E_U = 0.71$ V, $f = 100$ Hz, and with growth time $t_{\text{growth}} = 45$ min, in 0.2 mM PdCl₂ + 0.1 M HClO₄ solution. The surface facets were determined by comparing the average value of the interfacial angles of α with the theoretical ones³. The average value of interfacial angle α on the THH Pd NCs is measured to be 143.4°, which is close to the theoretical value of $\alpha = 143.1^\circ$ on a THH NC enclosed by {310} facets.

Table S2. Projections and geometrical parameters of THH nanocrystals.

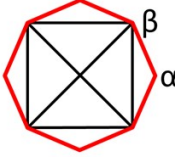
Polyhedral shape	Miller index	Projection direction	Projection	Character angel / degree
THH	$\{hk0\}$ ($h > k > 0$)	[001]		$\alpha = 2\arctan(\dots)$ $\beta = 270 - \alpha$

Table S3. Theoretical values of the interfacial angles of different facets on THH.

$\{hk0\}$	Angle	α
{11 3 0}		149.5°
{10 3 0}		146.6°
{310}		143.1°
{830}		138.9°
{730}		133.6°

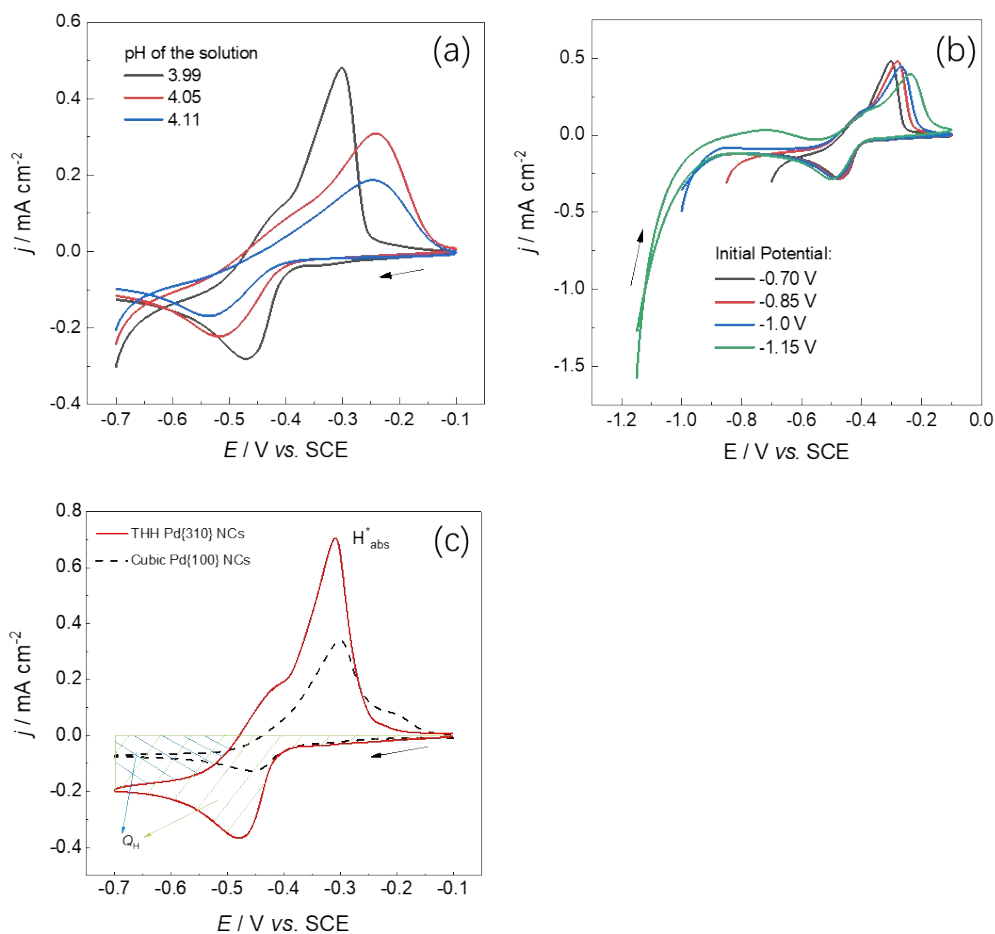


Figure S3. (a) CV features recorded on THH Pd{310} NCs/GC in 0.1 mol L⁻¹ Na₂SO₄ electrolyte at different pH. (b) CV features recorded on THH Pd{310} NCs/GC with different initial potentials in 0.1 mol L⁻¹ Na₂SO₄ at pH 4. (c) CV analysis on THH Pd{310} NCs/GC (in red) and cubic Pd{100} NCs/GC (in black) in 0.1 mol L⁻¹ Na₂SO₄ at pH 4. Scan rate: 50 mV s⁻¹.

The reduction and oxidation peaks between -0.7 V and -0.1V was pH sensitive since the peak currents significantly decreased as the solution pH slightly increase from 3.99 to 4.11. The more negatively lower potential was set, the more hydrogen was generated on the Pd surface, leading to the oxidation peak potential positively shifted. Above observations confirmed these reduction and oxidation peaks were corresponding to hydrogen adsorption and desorption process on THH Pd{310} NCs/GC and cubic Pd{100} NCs/GC. The charge density of hydrogen adsorption (the shadow area, Q_H) was then integrated in 0.1 M Na₂SO₄ solution at pH 4 and was about 2 mC cm⁻² for THH Pd{310} NCs/GC and 1.2 mC cm⁻² for cubic Pd{100} NCs/GC. The higher Q_H on the THH Pd{310} NCs/GC than that on the cubic Pd{100} NCs/GC indicated more adsorbed atomic hydrogen (H_{ads}^*) specie on THH Pd{310} NCs/GC.

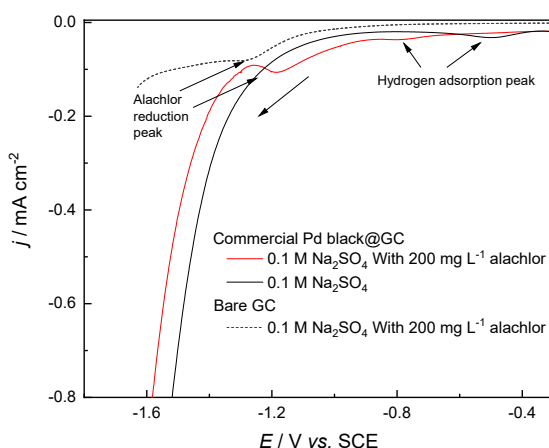


Figure S4. LSV of bare GC electrode in 200 ppm alachlor (in black dash) and comm. Pd black/GC with (in black dash) and without (in red solid) 200 ppm alachlor in 0.1 M Na_2SO_4 (pH=4). Scan rate: 10 mV s^{-1} .

Table S4. Removal efficiency and dechlorination selectivity of ECDR at $-1.0 \text{ V}_{\text{SCE}}$ of 0.2 mmol L^{-1} alachlor on the THH Pd{310} NCs/GC, cubic Pd{100} NCs/GC, and GC for 5h in 0.1 mol L^{-1} Na_2SO_4 at pH 4.

Pollutant	THH Pd{310} NCs/GC	Cubic Pd{100} NCs/GC	GC
R_{ala}	21.0%	20.3%	17.2%
S_{des}	6.6%	2.7%	2.3%

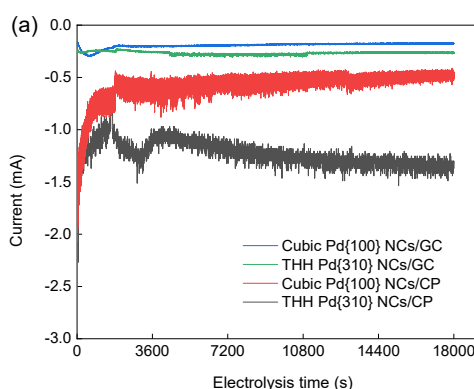


Figure S5. j - T plot on THH Pd{310} NCs and cubic Pd{100} NCs on GC or CP substrate, respectively, during constant-potential electrolysis of alachlor (@ -1.0 V) in 50 ppm alachlor in $0.1 \text{ M Na}_2\text{SO}_4$ (pH=4).

The LC-MS/MS analyses were conducted in the positive ionization mode on an ACE,

UltraCore 2.5 μ m C18 column. The gradient elution was regulated by water and acetonitrile at a flow rate of 0.35 mL/min as follows. 95% water and 5% acetonitrile isocratic elution were first used for 2 min, followed by a linear gradient to 70% acetonitrile within 30 min, and held at 70% acetonitrile for 10 min. The MS capillary temperature was 350 $^{\circ}$ C and the spray voltage was 3.5 kV. The injection volume was 20 μ L.

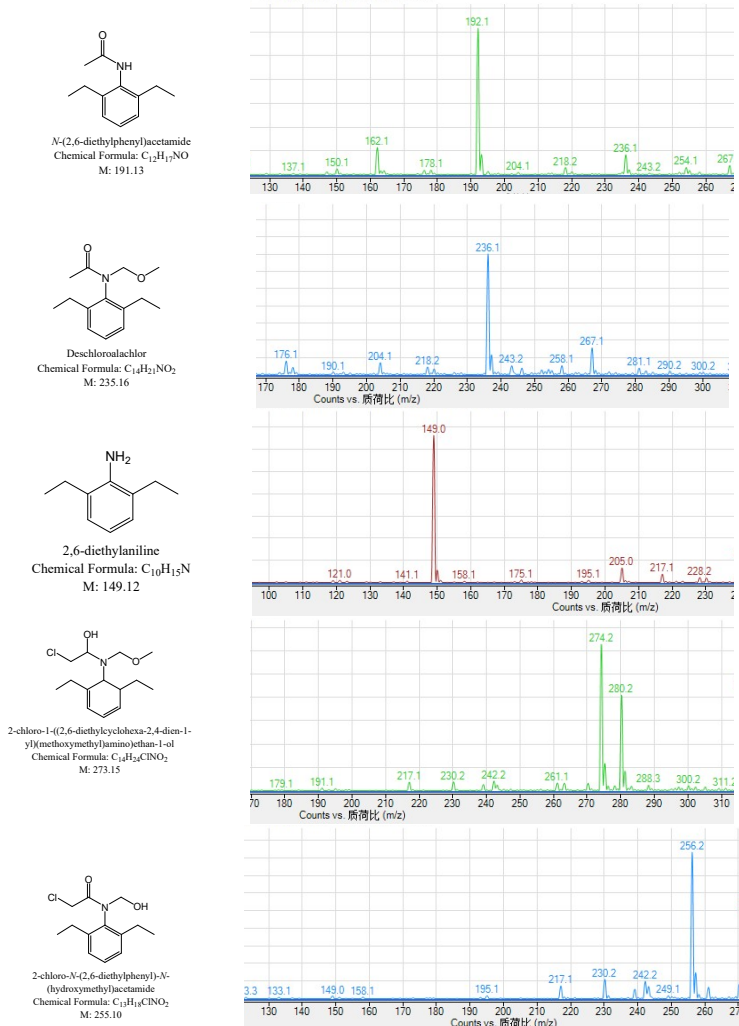


Figure S6. Mass spectra of alachlor degradation intermediates detected by LC-MS/MS

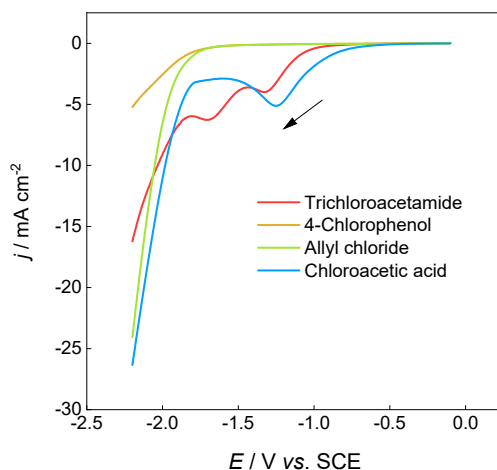
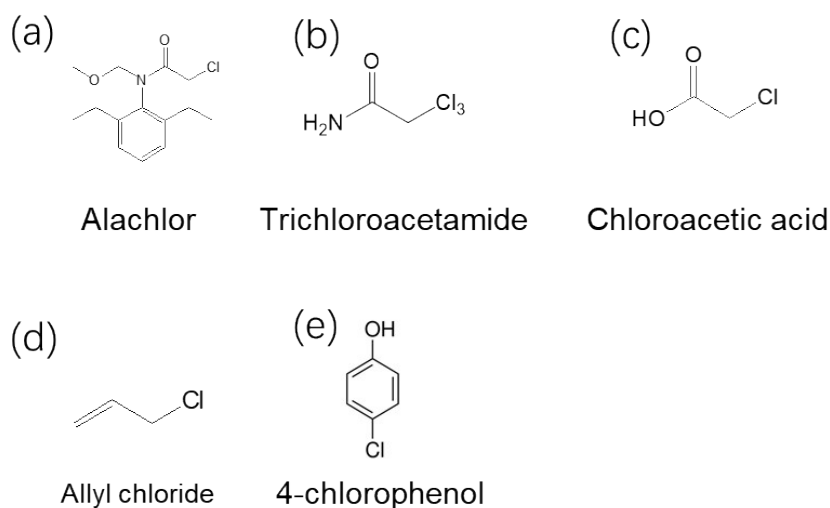


Figure S7. Linear sweep voltammetry (LSV) on glassy carbon with 20 mmol L⁻¹ allyl chloride, trichloroacetamide, trichloroacetic acid, 4-chlorophenol in 0.1 M Na₂SO₄ (pH=7), respectively. Scan rate: 10 mV s⁻¹.



Scheme S1. Structure of (a) alachlor, (b) trichloroacetamide, (c) chloroacetic acid, (d) allyl chloride, (e) 4-chlorophenol.

Table S5 Peak potential of studied compounds in 0.1 M Na₂SO₄ on THH Pd{310}NCs/GC, cubic Pd{100} NCs/GC, and comm. Pd black/GC and bare GC electrodes.

Pollutant	THH Pd{310} NCs/GC	Cubic Pd{100} NCs/GC	Pd black/GC	GC
Alachlor	-0.86	-1.03	-1.19	-1.28
Trichloroacetamid	-0.54	-0.51	-0.53	-1.32
e	-0.96	-1.13	-1.15	-1.70
	-1.21	-1.49	-1.48	--

Chloroacetic acid	-0.88	-1.36	-1.00	-1.23
Allyl chloride	-1.18	-1.31	-1.37	--
4-Chlorophenol	-0.86	-0.94	-1.09	--

-- No peak observed on GC electrode

Table S6 Assignments of IR bands appeared in the electrochemical *in-situ* FTIR spectra of alachlor reduction on THH Pd{310} NCs/GC. The shift of IR bands in spectra of cubic Pd{100} NCs/GC is indicated in the bracket.

IR band center / cm^{-1}	Direction of IR band	Assignments	dv/dE $\text{cm}^{-1} \text{V}^{-1}$	Ref.
1653 (0)	downward	stretching vibration of the amidic C=O group	36.7	4
1594 (--)	downward	H-down H_2O adsorbed on Pd	--**	5
1264 (--)*	downward	C-N stretching	--**	
1011 (7)	downward	C-O-C stretching	--**	6
1636 (--)*	upward	free H_2O	--**	
1225 (-13)	upward	asymmetrical stretching of HSO_4^-	--**	7
1152 (-5)	upward	C-C stretching	--**	8
1082 (-6)	upward	SO_4^{2-} stretching	--**	7

* Those bands were not seen on cubic Pd{100} NCs/GC.

**No shift was found

Density functional theory calculations

The constrained optimization approach is a much faster computational procedure for locating the transition state geometry. In this technique, the distance between two reacting atoms is set at a pre-selected value, which is determined by the choice of input geometry. By fixing the distance, but optimizing the geometry with respect to the remaining degrees of freedom, one can monitor the energy along the reaction coordinate by varying the constrained distance. The transition state could be identified (i) when the energy along the reaction coordinate is a maximum, but a minimum with respect to all the other remaining degrees of freedom, and (ii) the forces on the atoms vanish. Furthermore, diagonalization of the Hessian matrices for sampled structures has validated that this approach yields transition states with a single imaginary eigenvalue.

Reference

1. N. Tian, Z.-Y. Zhou, N.-F. Yu, L.-Y. Wang and S.-G. Sun, *Journal of the American Chemical Society*, 2010, **132**, 7580-7581.
2. S.-G. Sun, A.-C. Chen, T.-S. Huang, J.-B. Li and Z.-W. Tian, *J. Electroanal. Chem.*, 1992, **340**, 213-226.
3. R. R. Cui, Q. Shen, C. Y. Guo, B. Tang, N. J. Yang and G. H. Zhao, *Applied Catalysis B-Environmental*, 2020, **261**.
4. T. Sánchez-Verdejo, T. Undabeytia, S. Nir, J. Villaverde, C. Maqueda and E. Morillo, *J. Agric. Food Chem.*, 2008, **56**, 10192-10199.
5. J.-Y. Wang, H.-X. Zhang, K. Jiang and W.-B. Cai, *J. Am. Chem. Soc.*, 2011, **133**, 14876-14879.
6. Z.-Y. Zhou, D.-J. Chen, H. Li, Q. Wang and S.-G. Sun, *The Journal of Physical Chemistry C*, 2008, **112**, 19012-19017.
7. S.-G. Sun and Y. Lin, *Electrochimica Acta*, 1998, **44**, 1153-1162.
8. E. Segal, E. Haleva and A. Salomon, *ACS Applied Nano Materials*, 2019, **2**, 1285-1293.